PAPER

Hierarchically structured biphenylene-bridged periodic mesoporous organosilica†

Yan Li,[a] Andreas Keilbach,[a] Marcel Kienle,[a] Yasutomo Goto,[bc] Shinji Inagaki,[bc] Paul Knochel[a] and Thomas Bein*[a]

Novel composites of highly ordered and stable biphenyl-bridged periodic mesoporous organosilica (PMO) materials confined within the pores of anodic alumina membranes (AAM) were successfully synthesized by evaporation-induced self-assembly (EISA). 4,4′-Bis(triethoxysilyl)biphenyl (BTEBP) was used as a precursor in combination with the ionic surfactant cetyltrimethylammonium bromide (CTAB) or triblock-copolymer F127 as structure-directing agents. The resulting mesophases were characterized by small angle X-ray scattering (SAXS) and transmission electron microscopy (TEM). With ionic CTAB as a structure directing agent, samples with a mixture of the 2D-hexagonal columnar and a lamellar mesophase were obtained within the AAM channels. When using the nonionic surfactant F127, mesophases with a 2D-hexagonal circular structure were formed in the AAM channels. Additionally, a cubic $Im\bar{3}m$ phase could also be obtained with the same nonionic surfactant after the addition of lithium chloride to the precursor solution. The stability of both the circular and cubic biphenylene-bridged PMO against calcination temperatures of up to 250 °C was confirmed by NMR spectroscopy. Nitrogen sorption in the porous composite membrane shows typical type IV isotherms and narrow pore size distributions. All the biphenyl PMO/AAM composites show fluorescence due to the existence of biphenyl chromophores in the stable organosilica framework.

Introduction

The synthesis of periodic mesoporous organosilica (PMO) materials has attracted much interest since their discovery in 1999.[1–3] These materials can be synthesized from alkoxysilyl precursors $(RO)_3SiR'Si(OR)_3$ in the presence of surfactants such as tetraalkylammonium halides or nonionic copolymers acting as structure-directing agents. To date, numerous organic groups such as ethylene, thiophene, benzene, biphenylene, naphthalene, or divinylbenzene have been successfully incorporated in the framework of PMOs.[4–6] By varying the organic linker group R′, mesostructured materials tailored towards specific applications can be prepared. Such applications include catalysis,[7]

[a] Department of Chemistry and Center for NanoScience (CeNS), University of Munich (LMU), Butenandtstrasse 5–13 (E), Munich, 81377, Germany. E-mail: tbein@lmu.de; Fax: +49-89-2180-77622; Tel: +49-89-2180-77623

[b] Toyota Central R&D Laboratories Inc., Nagakute, Aichi, 480-1192, Japan. E-mail: inagaki@mosk.tytlabs.co.jp; Fax: +81-561-63-6507; Tel: +81-561-71-7393

[c] Core Research for Evolutional Science and Technology (CREST), Japan Science and Technology Agency (JST), Kawasaki, Saitama, 332-0012, Japan

† Electronic supplementary information (ESI) available: TEM micrographs of Bp-PMO samples, DFT pore-size distribution of the sample F127-circular-250 Bp-PMO, NMR spectra of the calcined F127-cubic-250 Bp-PMO. See DOI: 10.1039/c1jm12023a

adsorbents,[8] and optical[9,10] and electrical devices.[11] Recently, several PMO materials with optical properties have been reported, and among them, PMO thin films show interesting potential for use as fluorescent materials.[12–15] For example, Goto *et al.* investigated the fluorescence properties of aromatic-bridged PMO films and found that biphenyl-bridged PMO exhibited exceptionally high fluorescence quantum yield (0.45) compared with benzene-, naphthalene-, and anthracene-bridged PMO films (0.03–0.09).[12] A number of studies on biphenyl-bridged PMOs in powder form have been published.[16–23] Biphenyl-bridged PMO was also reported to exhibit excellent light-harvesting antenna properties[24] and to be applied to photocatalysis systems for hydrogen evolution from water[25] and CO_2 reduction to CO.[26]

As the biphenyl-bridged PMO materials have such promising catalytic and optical properties, preparing biphenyl PMO as films on surfaces or at interfaces would be beneficial for applications in fields such as nanoscale catalysts, gas sensors, and optical devices. In thin films, which are usually prepared on glass or silicon substrates, the alignment of the mesopore channels is most often parallel to the substrate surface.[12,27] However, for certain electrical or optical devices, further control over the mesopore orientation would be desirable.[28,29] Thus, there have been great efforts during the past few years to control the mesoporous domain size and orientation in mesoporous systems. These efforts include application of external electric[30,31] or magnetic fields,[32,33] or use of chemically[34,35] or lithographically[29]

17338 | *J. Mater. Chem.*, 2011, **21**, 17338–17344

This journal is © The Royal Society of Chemistry 2011

treated substrates. Among those methods, a feasible approach is to utilize anodic alumina membranes (AAMs) as host for mesoporous materials. For example, by incorporating mesostructured silica into the large channels of AAM, vertical alignment of the mesopores relative to the alumina membranes was achieved.[36–39] Moreover, these types of hierarchical nanostructures can offer significant advantages over self-supporting thin films, such as higher mechanical stability and high aspect ratios of the mesophase system. While inorganic mesoporous silica has been studied extensively in the confinement of AAM pores,[36–42] there are only a few reports on the synthesis of mesoporous organosilicas confined in AAM channels. Some of us have recently reported the synthesis of ethane-bridged PMO in anodic alumina membranes.[43] The observed mesophases include the 2D hexagonal circular, the lamellar, and the cubic $Im\bar{3}m$ phase. They are—except for the lamellar phase—stable against surfactant removal by solvent extraction or mild calcination protocols. It turned out to be far more challenging to obtain ordered mesostructures of siloxane precursors with the larger biphenylene bridges. This type of precursor shows low solubility and a high hydrolysis rate leading to almost instant precipitation under common synthesis conditions. While there are only a few reports on biphenylene-bridged PMO (Bp-PMO) thin films in the literature, we note that Bp-PMO thin films made with the ionic surfactant CTAB can show high order and stability.[44,45] However, thin films synthesized with block-copolymers under acidic conditions are usually not very stable against surfactant removal and are not highly ordered.[12] Given the favorable interaction of silica species with AAM channel walls found in inorganic silica/AAM systems, we reasoned that combining the biphenyl PMO system with AAMs might lead to different phase behavior and phase stability and thus open the way to designing novel hierarchical nanosystems which might move us closer to the application of Bp-PMO materials as optoelectronic devices.

In this study, we successfully synthesized highly ordered and stable Bp-PMO materials within AAM host systems. The synthesis was based on the evaporation-induced self-assembly (EISA) process.[46] Thus, 4,4′-bis(triethoxysilyl)biphenyl (BTEBP) was used as organosilica source in combination with CTAB and F127 as structure directing agents. The resulting hierarchical Bp-PMO systems were characterized by small angle X-ray scattering (SAXS), transmission electron microscopy (TEM), nitrogen sorption and nuclear magnetic resonance (NMR) spectroscopy. In contrast to Bp-PMO thin films, which were reported to be not highly ordered and also electron beam-sensitive,[12] Bp-PMO confined within AAM channels was found to be stable against calcination temperatures of up to 250 °C. The composite materials also showed good stability in the electron beam of the electron microscope. Furthermore, all the oriented Bp-PMO/AAM hierarchical materials showed fluorescence due to the existence of biphenyl chromophores in the stable organosilica framework.

Experimental section

Synthesis of siloxane precursor

4,4′-Bis(triethoxysilyl)biphenyl (BTEBP) was synthesized according to a procedure reported by Shea et al.[47] A dry and argon-flushed Schlenk-flask, equipped with a magnetic stirring bar and a septum, was charged with 4,4′-diiodobiphenyl (8.12 g, 20 mmol) and 40 mL THF. After cooling to 0 °C, iPrMgCl·LiCl (33.2 mL, 1.32 M in THF, 44 mmol) was added dropwise and stirred for 0.75 h. Then, the reaction mixture was cannulated to neat Si(OEt)$_4$ (20.8 g, 100 mmol) at 0 °C under argon. The mixture was allowed to warm up to 25 °C within 1.5 h. The crude reaction mixture was diluted with pentane (250 mL) and washed with NH$_4$Cl solution (5%, 100 mL). The organic layer was dried (MgSO$_4$), filtered, and concentrated under reduced pressure. Purification by flash chromatography (pentane/Et$_2$O, 9 : 1) yielded 4,4′-bis(triethoxysilyl)biphenyl (3.92 g, 41%) as a colorless oil. IR (ATR) ν (cm^{-1}) = 2974, 2925, 2886, 1600, 1389, 1295, 1165, 1128, 1094, 1070, 1004, 956, 807, 776, 732. ^{1}H NMR (300 MHz, CDCl$_3$) δ = 7.74 (d, ^3J(H,H) = 8.3 Hz, 4H, ArH), 7.62 (d, ^3J(H,H) = 8.3 Hz, 4H, ArH), 3.89 (q, ^3J(H,H) = 7.0 Hz, 12H, 6 × CH$_2$CH$_3$), 1.26 (q, ^3J(H,H) = 7.0 Hz, 18H, 6 × CH$_2$CH$_3$). ^{13}C NMR (75 MHz, CDCl$_3$) δ = 142.7, 135.3, 129.9, 126.6, 58.8, 18.3. HRMS (EI, m/z): calc. for [C$_{24}$H$_{38}$O$_6$Si$_2$] 478.2207, found: 478.2202.

Preparation of biphenylene-bridged PMO in AAM channels

The synthesis of Bp-PMO confined in AAM channels was achieved by the evaporation-induced self-assembly (EISA) approach. Whatman Anodiscs (47 mm and 25 mm diameter, nominal pore diameter 0.02 µm) were used as porous alumina substrates. SEM measurements showed that these membranes have an effective pore diameter between 150 and 250 nm. 4,4′-Bis (triethoxysilyl)biphenyl (BTEBP) served as organosilica precursor. The ionic surfactant cetyltrimethylammonium bromide (CTAB, Aldrich) as well as nonionic triblock-copolymer Pluronic F127 (Aldrich) were used as structure directing agents (SDA). All chemicals were used without further purification. In the following, the samples are named with the surfactant used followed by the description of the mesostructure formed, e.g. CTAB-columnar-lamellar indicates that the Bp-PMO within AAM channels is synthesized using CTAB as template and that it has a mesophase mixture of 2D-hexagonal columnar and lamellar structure.

For the preparation of the CTAB-columnar-lamellar sample, 0.060 g (0.125 mmol) of precursor BTEBP was mixed with 0.6 g of a 3.5 wt% ethanolic solution of CTAB (0.060 mmol) and stirred for 10 min. Then, 0.016 g (0.900 mmol) of distilled H$_2$O was added and the solution was stirred for an additional 10 min. Next, 2.75 µL of 0.1 M HCl (2.75 × 10^{-4} mmol) were added and the resulting solution was stirred for another 2 h. Finally, the AAM was placed on a Teflon plate and soaked with the above-prepared precursor solution by distributing 0.75 mL of the solution over the whole membrane surface (47 mm diameter). During the EISA-process, the ambient conditions were kept at 45–55% relative humidity and 25 °C.

For the preparation of the F127-circular hexagonal sample, the following, slightly altered protocol was used. First, Pluronic F127 (0.024 g, 0.002 mmol), ethanol (0.459 g), distilled H$_2$O (0.036 g, 2.0 mmol), and 1 M HCl (2.63 µL, 2.63 × 10^{-3} mmol) were added into a small glass vial and stirred for 1 h. Then, 0.060 g BTEBP (0.125 mmol) was added to this solution and stirred for 3 min. Afterwards, a volume of 0.2 mL of the above

prepared solution was cast onto the AAM surface (25 mm diameter) and left to dry. During this EISA-process, the ambient conditions were kept at 25–28% relative humidity and 25 °C. The synthesis conditions of the F127-cubic sample followed the same protocol as above, except that 0.0024 g LiCl (0.056 mmol) was additionally added to the F127 solution and only 0.10 mL of solution were cast onto the AAM surface (25 mm diameter).

If samples were calcined, the heating rate was 0.5 °C min⁻¹ below 200 °C and 0.25 °C min⁻¹ from 200 °C to 250 °C. The annealing periods were 5 h at 120 °C, 5 h at 200 °C and finally 10 h at 250 °C.

Characterization

The samples were characterized with 2D small-angle X-ray scattering (SAXS) using the SAXSess system by Anton Paar in combination with a CCD detector system (Roper Scientific). The wavelength of the incident beam is 0.1541 nm (Cu Kα), the sample–detector distance was set to 308 mm. Samples were measured with a tilt angle of 10° with respect to the primary beam. Transmission electron microscopy (TEM) was performed using a JEOL 2011 with an acceleration voltage of 200 kV. Nitrogen sorption measurements were carried out at −196 °C using an Autosorb-1 by Quantachrome Instruments and before the measurements, the samples were degassed at 150 °C for 12 h in vacuum. The Brunauer–Emmett–Teller (BET) surface area was calculated using experimental points at a relative pressure range of $p/p_0 = 0.05–0.20$. The total pore volume was calculated by the N_2 amount adsorbed at the highest p/p_0 ($p/p_0 = 0.95$). DFT pore size distributions were calculated using a SiO_2 kernel assuming a cylindrical pore geometry for the F127-circular hexagonal sample and a cylindrical/sphere pore geometry for the F127-cubic sample. Solid-state ^{13}C and ^{29}Si NMR measurements were performed using a Bruker Avance III 500 spectrometer. The fluorescence spectra were measured with a fluorescence spectroscopy system (PTI 814 from Photon Technology international) with a xenon arc lamp.

Results and discussion

CTAB-columnar-lamellar Bp-PMO

Using the ionic surfactant cetyltrimethylammonium bromide (CTAB) as structure directing agent, a phase mixture of the hexagonal columnar and the lamellar phase was obtained within the AAM channels. This can be contrasted to our previous results on CTAB/ethane-bridged PMO/AAM composites that form a 2D-hexagonal circular mesophase.[43] This difference could be related to the different character of the organic bridges of the siloxane precursor, such as the hydrophobicity, the flexibility and the size of the bridges, which might lead to different interactions between the SDA (structure directing agents) and the organosilane precursor and thus lead to the formation of different mesophases. 2D small angle X-ray scattering (2D-SAXS) and transmission electron microscopy (TEM) were performed to characterize the mesostructure of the CTAB-columnar-lamellar system. The 2D-SAXS diffraction pattern for this confined Bp-PMO system (Fig. 1A) shows only in-plane diffractions that correspond to either the hexagonal columnar phase or the lamellar structure.
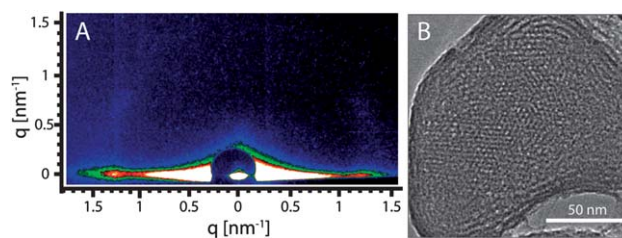

Fig. 1 (A) 2D-SAXS pattern and (B) plane-view TEM micrograph of the as-prepared CTAB-columnar-lamellar sample representing a mesophase mixture of the columnar and lamellar structure.

The observed *d*-spacing covers a wide range from 3.7 nm to 5.2 nm. According to previous studies, it is generally possible to distinguish between in-plane diffraction corresponding to the hexagonal phase or to the lamellar structure, as their *d*-values differ by a factor of sin (120°).[40] The diffraction spots corresponding to a larger *d*-spacing (closer to the primary beam) can be assigned to the lamellar phase, and the smaller *d*-spacing is assigned to the columnar phase, respectively. Additionally, TEM micrographs of the as-prepared CTAB-columnar-lamellar Bp-PMO system confirm the formation of the phase mixture of columnar and lamellar structures. Plane-view TEM micrographs of such samples show that the lamellar phase is preferentially located at the AAM channel wall surrounding the columnar hexagonal phase in the center of the channel (Fig. 1B). Because of the lamellar structure existing in the system, the mesophase of the CTAB-columnar-lamellar system is not stable after surfactant removal due to the lack of 3-dimensional connection of the lamellar phase. In this case, obtaining good micrographs was difficult because of the shrinkage of the lamellar structure caused by electron beam irradiation (Fig. S1†).

F127-circular Bp-PMO

A second mesophase configuration was realized by using the nonionic surfactant pluronic F127 as structure directing agent. Bp-PMO with a 2D-hexagonal circular mesostructure was formed in AAM channels. The diffraction pattern recorded from 2D-SAXS measurements (Fig. S2A†) for the as-prepared F127-circular sample shows both in-plane and out-of-plane reflections that can be assigned to a circular hexagonal structure.[42,43] In order to obtain an open pore system, the sample was calcined in air at 250 °C for 10 h to remove the surfactant template molecules from the mesophase. After calcination, the F127-circular-250 Bp-PMO (F127-circular sample calcined at 250 °C) features a highly ordered mesostructure as observed by 2D-SAXS (Fig. 2A). The average *d*-spacing calculated from the diffraction pattern is 12.8 nm, which is in agreement with corresponding TEM results (Fig. 2B). TEM micrographs of calcined samples also confirmed the preservation of the highly ordered and stable Bp-PMO with a minor shrinkage in the AAM channels after calcination (Fig. S2B†).

The nitrogen sorption isotherms (Fig. 3) of F127-circular-250 Bp-PMO show the typical type IV isotherm shape commonly observed for mesoporous materials, as well as a hysteresis loop.

The BET surface area calculated from these isotherms is 58 m² g⁻¹ and the pore volume is 0.072 mL g⁻¹ (the mass includes the
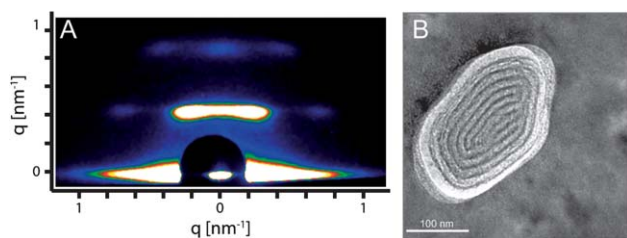
17340 | *J. Mater. Chem.*, 2011, **21**, 17338–17344

This journal is © The Royal Society of Chemistry 2011

Fig. 2 (A) 2D-SAXS pattern and (B) plan-view TEM micrograph showing the highly ordered circular structure of a calcined sample F127-circular-250.
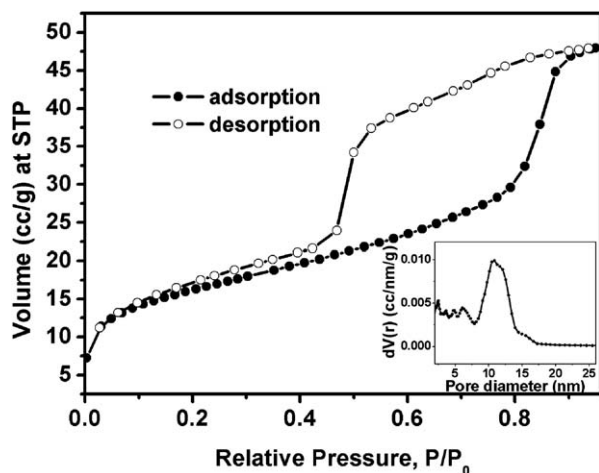

Fig. 3 Nitrogen adsorption (●) and desorption (○) isotherms of the sample F127-circular-250 Bp-PMO with an inset showing the corresponding pore size distribution calculated by a DFT model from the adsorption branch.

Fig. 4 (A) ^{13}C-MAS NMR and (B) ^{29}Si NMR spectra of the calcined F127-circular-250 Bp-PMO sample.

AAM membrane), which are both similar to other previously reported values for PMO/AAM composites.[43] The isotherm shape (hysteresis loop) suggests the existence of ink-bottle shaped pores. This can be confirmed by comparing the DFT pore-size distribution from the adsorption branch (av. pore diameter ~10.5 nm) and the desorption branch (av. pore diameter ~5 nm), both of which show sharp pore size distributions with no significant distribution of the pore entrance sizes visible (Fig. S3†). The ^{13}C-MAS NMR spectrum (Fig. 4A) shows that the biphenylene groups are intact in the calcined material. The four aromatic resonances and their side bands are consistent with the results reported for the plain Bp-PMO system.[16,19] In addition, there is a weak signal that can be assigned to residual F127 molecules, indicating that the removal of the template is not yet fully completed after these calcination conditions. In the ^{29}Si NMR spectrum of the calcined F127-circular-250 sample (Fig. 4B), we observe strong resonances with high intensity attributed to T²-silicon species (CSi(OSi)$_2$(OH)) at −70.8 ppm and T³ species (CSi(OSi)$_3$) at −78.8 ppm. We note that only a minor resonance appears around −99.7 ppm; this signal can be assigned to Q³ sites,[48] indicating that most of the Si–C bonds in the framework of the Bp-PMO material are still intact after calcination in air at 250 °C. Compared to Bp-PMO thin films, which were reported to be not highly ordered and electron beam sensitive,[12] the F127-circular Bp-PMO system within AAM
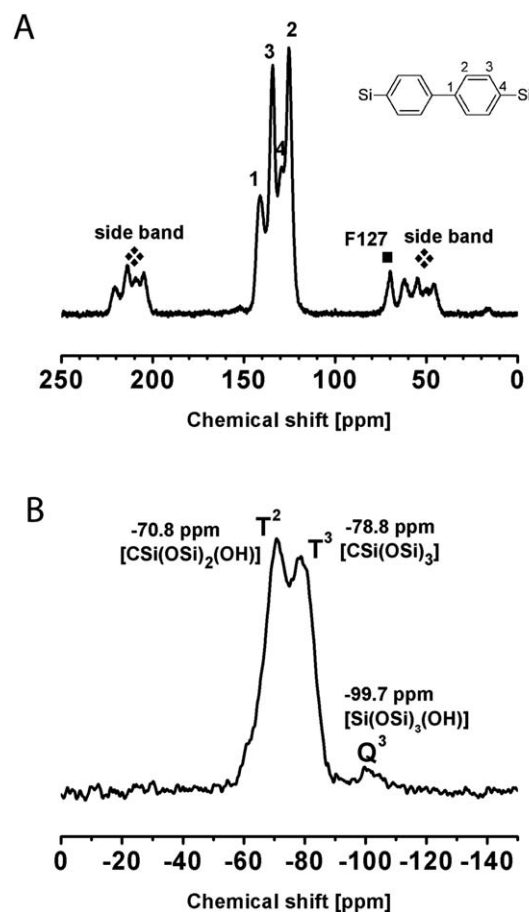
channels shows a well-ordered mesopore system with high thermal and electron beam stability. We note that the same synthesis mixture did not result in an ordered mesostructure when deposited as thin film on a glass substrate.

F127-cubic Bp-PMO

Several recent reports have pointed to the profound impact of metal salts on the phase behavior of the surfactant-templated mesoporous silica, which was described as "salt-induced phase transformation".[49–54] In an effort to study this effect in our Bp-PMO/AAM systems, we added inorganic salt to the synthesis solution for the F127-circular Bp-PMO system in order to possibly induce a transformation of the hexagonal circular to another mesophase. Lithium chloride was chosen as the inorganic additive because of its significant effect on the micellar hydration and gelation behavior of PEO–PPO–PEO triblock copolymers in solution.[55,56] The added LiCl indeed had a striking impact on the phase behavior, as the resulting PMO/AAM composites now showed a mesophase with the cubic $Im\bar{3}m$ structure (body centered cubic), which is different from the original 2D hexagonal circular mesophase obtained without salt addition. The 2D-SAXS pattern of F127-cubic-200 Bp-PMO (F127-cubic sample calcined at 200 °C) shows the typical reflections assigned to the cubic $Im\bar{3}m$ phase (Fig. 5A), similar to
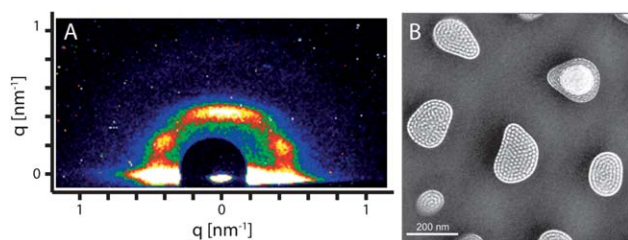
Fig. 5 (A) 2D-SAXS pattern and (B) plan-view TEM of the F127-cubic-200 sample representing a highly ordered cubic structure with the absence of shrinkage after calcination at 200 °C.

recent observations with other PMO and mesoporous polymer phases in AAM hosts.[43,57] The formation of a cubic mesostructure was also confirmed by the following TEM micrographs. A plan-view TEM micrograph obtained from F127-cubic-200 Bp-PMO is displayed in Fig. 5B. Two orientations, one along [111] (Fig. S4A†) and the other along [110] (Fig. S4B†), can be observed. It is noteworthy that even after calcination at 200 °C, the sample shows no shrinkage, which is consistent with the low shrinkage of other cubic mesophases confined in AAM.[43] Another reason for the absence of shrinkage might be the added inorganic ions, which have been observed to increase the chemical interactions between organic silica mesophases and the AAM channel surface.[55] The nitrogen sorption isotherm (Fig. 6) of F127-cubic-250 Bp-PMO (F127-cubic sample calcined at 250 °C) shows the type IV shape with a broad hysteresis loop that is attributed to the existence of bottlenecks connecting pores in the cubic system. The F127-cubic-250 sample shows a BET surface area of 44 $m^2 g^{-1}$ and a pore volume of 0.053 mL g^{-1}, comparable with the values obtained from the circularly structured system F127-circular-250 described above. The pore-size distribution peaks at a pore diameter of 13.8 nm. The ^{13}C and ^{29}Si NMR data (Fig. S5†) of the sample F127-cubic-250 Bp-PMO are consistent with those obtained from the sample F127-circular-250 Bp-PMO. The cubic $Im\bar{3}m$ structured Bp-PMO material shows a well-ordered mesophase and thermal stability up to 250 °C, which is advantageous for possible
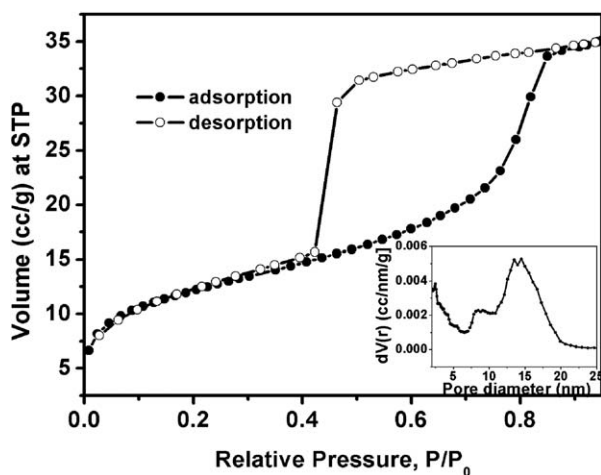

Fig. 6 Nitrogen adsorption (●) and desorption (○) isotherms of the F127-cubic-250 Bp-PMO with an inset showing the corresponding pore size distribution calculated by a DFT model from the adsorption branch.
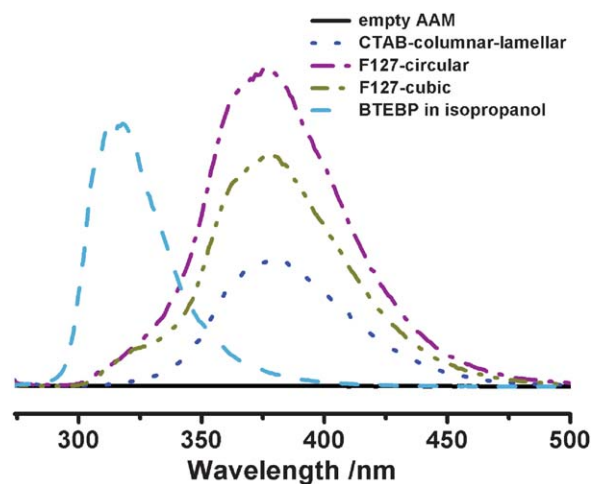

Fig. 7 Fluorescent spectra (excited at 266 nm) of as-prepared Bp-PMO phases within AAM channels and a diluted BTEBP precursor solution in isopropanol (10^{-5} M) (the intensities are not to scale).

applications of these Bp-PMO materials. We attribute the phase transformation from the 2D hexagonal circular phase to the $Im\bar{3}m$ cubic phase upon the addition of LiCl to the following mechanism. The presence of Li$^+$ ions and Cl$^-$ ions can change the micellar hydration behavior of the pluronic F127 solution and thus change the curvature of the micelles.[55,56,58,59] Specifically, on the one hand, the Cl$^-$ ion has the effect of dehydrating hydrophilic groups of F127 micelles and thus decreasing the curvature of F127 micelles. On the other hand, hydrated Li$^+$ ions can form complexes with the PEO chains in the micellar corona region,[58–60] which can enlarge the hydrophilic head groups of the F127 micelles. In general, the effect of hydrated Li$^+$ is stronger than that of Cl$^-$, such that the size of the hydrophilic head groups of F127 micelles can be increased, which can lead to more hydrophilic F127 micelles with higher curvature. Thus, we propose that the body-centered cubic $Im\bar{3}m$ structure with a higher micellar curvature was obtained after addition of LiCl to a solution that originally would result in the 2D hexagonal (circular) structure.

Fluorescent properties

Fig. 7 shows fluorescence spectra of all the Bp-PMO phases within AAM channels and of a diluted solution of the BTEBP precursor. The fluorescence bands of all the Bp-PMO phases are shifted significantly to longer wavelengths compared to the emission wavelength of the diluted pure precursor solution. This emission behavior is consistent with that of the Bp-PMO thin film on quartz surfaces reported by Goto *et al.*,[12] indicating strong electronic interactions between the aromatic biphenyl groups that exist in the Bp-PMO phases in the AAM channels.

Conclusions

In summary, different PMO mesophases based on the biphenylene-bridged ethoxysilane BTEBP were successfully synthesized through an evaporation-induced self-assembly (EISA)-process within the pores of anodic alumina membranes. Depending on the surfactant used, different mesophases (Bp-PMO) could be observed. Using CTAB as the structure-directing surfactant,

2D-SAXS experiments and TEM images showed that a phase mixture of the 2D-hexagonal columnar and the lamellar meso-structure was formed (sample CTAB-columnar-lamellar Bp-PMO). The lamellar phase appears to be preferentially located close to the alumina walls, while the hexagonal columnar phase is dominant in the center of the channels. This result contrasts with earlier findings for CTAB/ethane-bridged PMO/AAM compos-ites, where a hexagonal circular phase was the only mesophase obtained. When using the block-copolymer F127 as structure directing agent, the hexagonal circular PMO structure was found in the confined environment of the AAM pores. The addition of LiCl to the precursor/F127 solution leads to a striking structural transformation from the hexagonal circular to the body centered cubic ($Im\bar{3}m$) mesophase. The resulting composites with circular and cubic mesophases were both structurally stable against calcination in air at temperatures of up to 250 °C, which was also confirmed by ^{13}C and ^{29}Si NMR measurements. All the prepared Bp-PMO/AAM hierarchical nanostructures showed fluorescence due to the biphenyl chromophores in the organosilica frame-work. The energy shift of the fluorescence emission with respect to the precursor molecules points to strong electronic interac-tions of the chromophores in the confined organosilica network. We therefore anticipate that the stable and oriented Bp-PMO/AAM composites and similar ordered chromophore-containing mesoporous hierarchical nanostructures will offer promise as optoelectronic systems.

Acknowledgements

References

1 T. Asefa, M. J. MacLachlan, N. Coombs and G. A. Ozin, *Nature*, 1999, **402**, 867–871.
2 S. Inagaki, S. Guan, Y. Fukushima, T. Ohsuna and O. Terasaki, *J. Am. Chem. Soc.*, 1999, **121**, 9611–9614.
3 B. J. Melde, B. T. Holland, C. F. Blanford and A. Stein, *Chem. Mater.*, 1999, **11**, 3302–3308.
4 B. Hatton, K. Landskron, W. Whitnall, D. Perovic and G. A. Ozin, *Acc. Chem. Res.*, 2005, **38**, 305–312.
5 F. Hoffmann, M. Cornelius, J. Morell and M. Fröba, *Angew. Chem., Int. Ed.*, 2006, **45**, 3216–3251.
6 B. D. Hatton, K. Landskron, W. Whitnall, D. D. Perovic and G. A. Ozin, *Adv. Funct. Mater.*, 2005, **15**, 823–829.
7 Q. H. Yang, J. Liu, L. Zhang and C. Li, *J. Mater. Chem.*, 2009, **19**, 1945–1955.
8 V. Rebbin, R. Schmidt and M. Fröba, *Angew. Chem., Int. Ed.*, 2006, **45**, 5210–5214.
9 P. N. Minoofar, R. Hernandez, S. Chia, B. Dunn, J. I. Zink and A. C. Franville, *J. Am. Chem. Soc.*, 2002, **124**, 14388–14396.
10 R. Hernandez, A. C. Franville, P. Minoofar, B. Dunn and J. I. Zink, *J. Am. Chem. Soc.*, 2001, **123**, 1248–1249.
11 N. Mizoshita, M. Ikai, T. Tani and S. Inagaki, *J. Am. Chem. Soc.*, 2009, **131**, 14225–14227.
12 Y. Goto, N. Mizoshita, O. Ohtani, T. Okada, T. Shimada, T. Tani and S. Inagaki, *Chem. Mater.*, 2008, **20**, 4495–4498.
13 N. Mizoshita, Y. Goto, T. Tani and S. Inagaki, *Adv. Funct. Mater.*, 2008, **18**, 3699–3705.
14 N. Mizoshita, Y. Goto, T. Tani and S. Inagaki, *Adv. Mater.*, 2009, **21**, 4798–4801.
15 N. Mizoshita, Y. Goto, Y. Maegawa, T. Tani and S. Inagaki, *Chem. Mater.*, 2010, **22**, 2548–2554.
16 M. P. Kapoor, Q. H. Yang and S. Inagaki, *J. Am. Chem. Soc.*, 2002, **124**, 15176–15177.
17 J. Morell, C. V. Teixeira, M. Cornelius, V. Rebbin, M. Tiemann, H. Amenitsch, M. Fröba and M. Linden, *Chem. Mater.*, 2004, **16**, 5564–5566.
18 Y. Yang and A. Sayari, *Chem. Mater.*, 2007, **19**, 4117–4119.
19 M. P. Kapoor, Q. H. Yang, Y. Goto and S. Inagaki, *Chem. Lett.*, 2003, 914–915.
20 M. Park, S. S. Park, M. Selvaraj, D. Y. Zhao and C. S. Ha, *Microporous Mesoporous Mater.*, 2009, **124**, 76–83.
21 K. J. Balkus, T. J. Pisklak, G. Hundt, J. Sibert and Y. F. Zhang, *Microporous Mesoporous Mater.*, 2008, **112**, 1–13.
22 E. R. Magdaluyo, R. V. R. Virtudazo, L. P. dela Cruz, E. V. Castriciones and H. D. Mendoza, *J. Ceram. Process. Res.*, 2010, **11**, 15–19.
23 F. Hoffmann, M. Guengerich, P. J. Klar and M. Fröba, *J. Phys. Chem. C*, 2007, **111**, 5648–5660.
24 S. Inagaki, O. Ohtani, Y. Goto, K. Okamoto, M. Ikai, K. Yamanaka, T. Tani and T. Okada, *Angew. Chem., Int. Ed.*, 2009, **48**, 4042–4046.
25 M. Ohashi, M. Aoki, K. I. Yamanaka, K. Nakajima, T. Ohsuna, T. Tani and S. Inagaki, *Chem.–Eur. J.*, 2009, **15**, 13041–13046.
26 H. Takeda, M. Ohashi, T. Tani, O. Ishitani and S. Inagaki, *Inorg. Chem.*, 2010, **49**, 4554–4559.
27 S. Y. Wu, H. S. Hsueh and M. H. Huang, *Chem. Mater.*, 2007, **19**, 5986–5990.
28 Y. N. Xia, P. D. Yang, Y. G. Sun, Y. Y. Wu, B. Mayers, B. Gates, Y. D. Yin, F. Kim and Y. Q. Yan, *Adv. Mater.*, 2003, **15**, 353–389.
29 R. L. Rice, D. C. Arnold, M. T. Shaw, D. Iacopina, A. J. Quinn, H. Amenitsch, J. D. Holmes and M. A. Morris, *Adv. Funct. Mater.*, 2007, **17**, 133–141.
30 M. Trau, N. Yao, E. Kim, Y. Xia, G. M. Whitesides and I. A. Aksay, *Nature*, 1997, **390**, 674–676.
31 K. Kuraoka, Y. Tanaka, M. Yamashita and T. Yazawa, *Chem. Commun.*, 2004, 1198–1199.
32 A. Firouzi, D. J. Schaefer, S. H. Tolbert, G. D. Stucky and B. F. Chmelka, *J. Am. Chem. Soc.*, 1997, **119**, 9466–9477.
33 Y. Yamauchi, M. Sawada, T. Noma, H. Ito, S. Furumi, Y. Sakka and K. Kuroda, *J. Mater. Chem.*, 2005, **15**, 1137–1140.
34 H. Miyata, T. Noma, M. Watanabe and K. Kuroda, *Chem. Mater.*, 2002, **14**, 766–772.
35 H. Miyata, T. Suzuki, A. Fukuoka, T. Sawada, M. Watanabe, T. Noma, K. Takada, T. Mukaide and K. Kuroda, *Nat. Mater.*, 2004, **3**, 651–656.
36 Z. L. Yang, Z. W. Niu, X. Y. Cao, Z. Z. Yang, Y. F. Lu, Z. B. Hu and C. C. Han, *Angew. Chem., Int. Ed.*, 2003, **42**, 4201–4203.
37 A. Yamaguchi, F. Uejo, T. Yoda, T. Uchida, Y. Tanamura, T. Yamashita and N. Teramae, *Nat. Mater.*, 2004, **3**, 337–341.
38 B. Platschek, N. Petkov and T. Bein, *Angew. Chem., Int. Ed.*, 2006, **45**, 1134–1138.
39 A. Yamaguchi, H. Kaneda, W. S. Fu and N. Teramae, *Adv. Mater.*, 2008, **20**, 1034–1037.
40 B. Platschek, R. Köhn, M. Döblinger and T. Bein, *Langmuir*, 2008, **24**, 5018–5023.
41 A. Y. Ku, S. T. Taylor and S. M. Loureiro, *J. Am. Chem. Soc.*, 2005, **127**, 6934–6935.
42 B. Platschek, R. Köhn, M. Döblinger and T. Bein, *ChemPhysChem*, 2008, **9**, 2059–2067.
43 A. Keilbach, M. Döblinger, R. Köhn, H. Amenitsch and T. Bein, *Chem.–Eur. J.*, 2009, **15**, 6645–6650.
44 M. A. Wahab and C. B. He, *J. Nanosci. Nanotechnol.*, 2008, **8**, 6381–6386.
45 M. A. Wahab and C. B. He, *Langmuir*, 2009, **25**, 832–838.
46 C. J. Brinker, Y. F. Lu, A. Sellinger and H. Y. Fan, *Adv. Mater.*, 1999, **11**, 579–585.
47 K. J. Shea, D. A. Loy and O. Webster, *J. Am. Chem. Soc.*, 1992, **114**, 6700–6710.
48 C. Breen, J. Madejova and P. Komadel, *J. Mater. Chem.*, 1995, **5**, 469–474.
49 Y. X. Yang, X. P. Qu, Y. R. Chen, X. C. Jia, J. B. Zhang and X. N. Liu, *J. Am. Ceram. Soc.*, 2007, **90**, 2050–2056.
50 C. Z. Yu, B. Z. Tian, J. Fan, G. D. Stucky and D. Y. Zhao, *Chem. Commun.*, 2001, 2726–2727.
51 C. Z. Yu, B. Z. Tian, J. Fan, G. D. Stucky and D. Y. Zhao, *J. Am. Chem. Soc.*, 2002, **124**, 4556–4557.
52 K. Flodstrom, V. Alfredsson and N. Kallrot, *J. Am. Chem. Soc.*, 2003, **125**, 4402–4403.

This journal is © The Royal Society of Chemistry 2011

J. Mater. Chem., 2011, **21**, 17338–17344 | 17343

53 J. W. Tang, C. Z. Yu, X. F. Zhou, X. X. Yan and D. Y. Zhao, *Chem. Commun.*, 2004, 2240–2241.

54 M. Okamoto, Y. Fukukita, M. Haga, K. Toyofuku and N. Mimura, *J. Porous Mater.*, 2009, **16**, 135–140.

55 B. Platschek, N. Petkov, D. Himsl, S. Zimdars, Z. Li, R. Köhn and T. Bein, *J. Am. Chem. Soc.*, 2008, **130**, 17362–17371.

56 R. Ganguly and V. K. Aswal, *J. Phys. Chem. B*, 2008, **112**, 7726–7731.

57 J. Schuster, A. Keilbach, M. Döblinger and T. Bein, *Chem.–Eur. J.*, 2011, **17**, 9463–9470.

58 J. J. Lin and I. J. Cheng, *J. Appl. Polym. Sci.*, 2002, **85**, 612–621.

59 Y. Q. Wang, Y. J. Wang, C. M. Yang, G. Z. Lu and F. Schüth, *Langmuir*, 2006, **22**, 5491–5496.

60 P. Alexandridis and J. F. Holzwarth, *Langmuir*, 1997, **13**, 6074–6082.